

Electronic Supplementary Information:
Electrostatically Driven Drumhead Resonators
Based on Freestanding Membranes of
Cross-Linked Gold Nanoparticles

Hendrik Schlicke,^{†,‡} Clemens J. Schröter,^{†,‡} and Tobias Voßmeyer^{*,†}

*Institute of Physical Chemistry, University of Hamburg, Grindelallee 117, 20146 Hamburg,
Germany*

E-mail: tobias.voßmeyer@chemie.uni-hamburg.de

^{*}To whom correspondence should be addressed

[†]Institute of Physical Chemistry, University of Hamburg, Grindelallee 117, 20146 Hamburg, Germany

[‡]Contributed equally to this work.

Gold Nanoparticles

Transmission electron microscopy was used for the determination of the GNPs' average size and size distribution. As the 1-dodecylamine stabilized particles were not stable under TEM conditions, the amine ligands were exchanged with stronger binding 1-dodecanethiol (12T) ligands, as described earlier.¹ The 12T stabilized particles were drop-casted onto a carbon coated TEM substrate and investigated using a JEOL JEM-1011 transmission electron microscope, equipped with a LaB₆ cathode operated at 100 kV.

Figure S1 shows a representative transmission electron micrograph of the particle batch used for preparing the GNP membranes, as well as a size histogram. An average diameter of 3.6 ± 0.6 nm was determined. Particles with diameters < 1 nm were excluded from the sizing statistics.

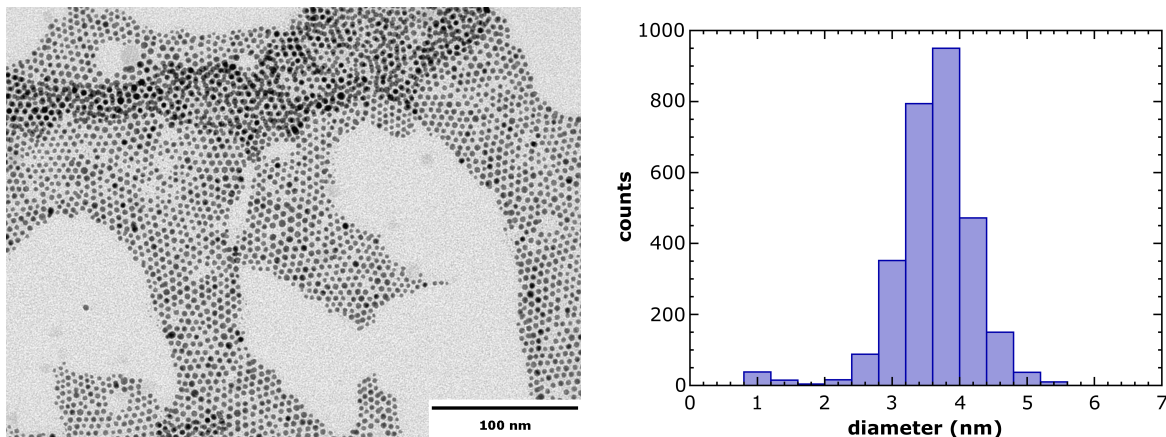


Figure S1: Transmission electron micrograph (left) and size histogram (right) of the GNP batch used for membrane fabrication.

UV/vis Spectroscopy

All membranes used for device fabrication were characterized regarding their UV/vis absorption. Figure S2 shows UV/vis absorbance spectra of the diluted GNP stock solution in n-heptane (dilution factor $f = 1/600$) and the as-deposited 6DT cross-linked GNP films on glass substrates prior to lift-off and transfer. A pronounced surface plasmon absorbance band originating from the GNPs within the membranes is observed. Compared to the solution phase spectrum, the plasmon band is red shifted due to the short interparticle distances resulting in plasmonic interactions.

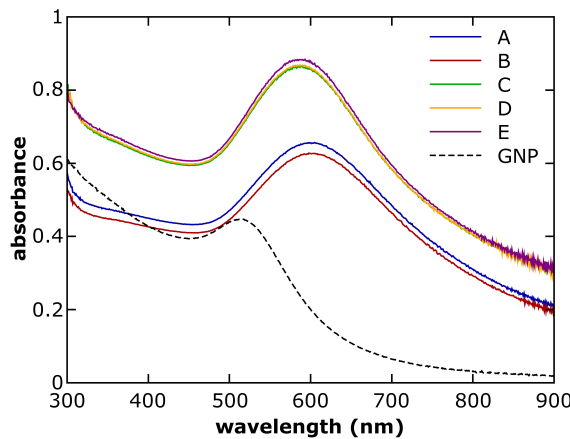


Figure S2: UV/vis absorbance spectrum of the GNP stock solution in n-heptane (dilution factor $f = 1/600$, dashed black line) and UV/vis absorbance spectra of the GNP films used for fabrication of devices A, B, C, D and E (see table S1).

Film Thickness Measurements (AFM)

Five 6DT cross-linked GNP membranes were used for device fabrication in this study. The thickness of the membranes was determined by atomic force microscopy (AFM). Sections of the as-deposited films on glass substrates were scratched using a cannula and AFM scans ($5 \times 20 \mu\text{m}^2$, $128 \times 512 \text{ px}^2$) were recorded at the edges of the resulting scratches. Two AFM scans were recorded at different positions on each sample. The scans are depicted in figure S3. From each scan, 4 line profiles were extracted and the step heights were averaged. Table S1 presents the thicknesses of the membranes used for resonator fabrication.

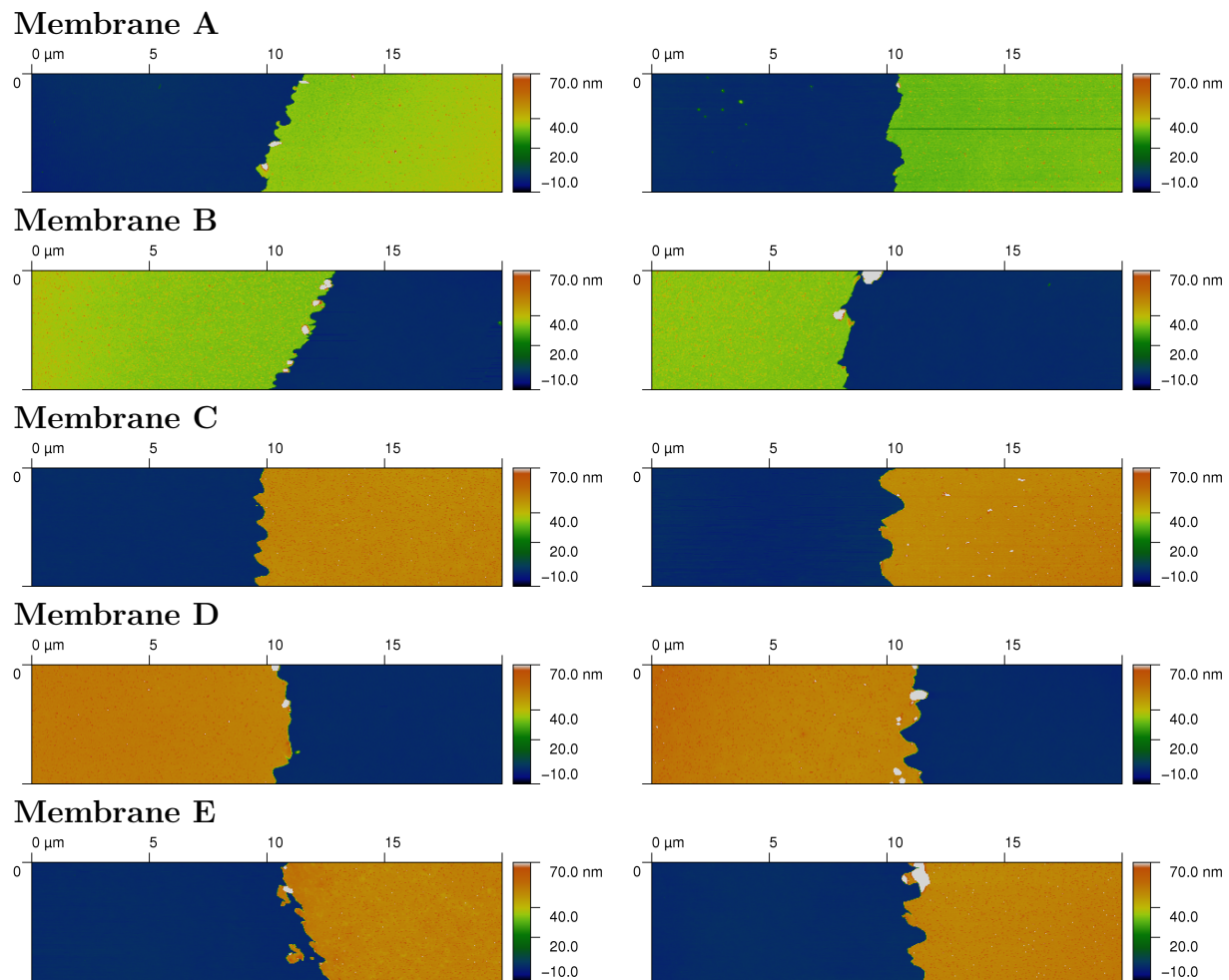


Figure S3: AFM scans ($20 \times 5 \mu\text{m}^2$) of GNP film sections used for thickness measurements. These films were used for fabricating the resonator devices A, B, C, D and E. The extracted film thicknesses are provided in table S1.

Charge Transport Measurements

Sections of the substrate-supported GNP-films were investigated regarding their charge transport properties. For this purpose, gold electrodes (thickness: ~ 100 nm) were deposited onto the as-prepared GNP films by vacuum evaporation using a cannula (0.4 mm diameter) as a shadow mask. Current-voltage (IV) curves were recorded by contacting the samples using microprobes in a custom-built probe station and sweeping the voltage in a range between -5 and 5 V using an Agilent 4156C semiconductor parameter analyzer. All samples showed ohmic behavior. IV data (normalized to a channel width of 1 cm and channel length of 400 μ m) of the membranes used for device fabrication in this study are plotted in figure S4. The higher currents measured for the films C, D and E with respect to A and B result from their higher thickness. Taking into account the film thickness, all films showed a conductivity of 0.1 S cm^{-1} , which is in good agreement with earlier studies.¹⁻³

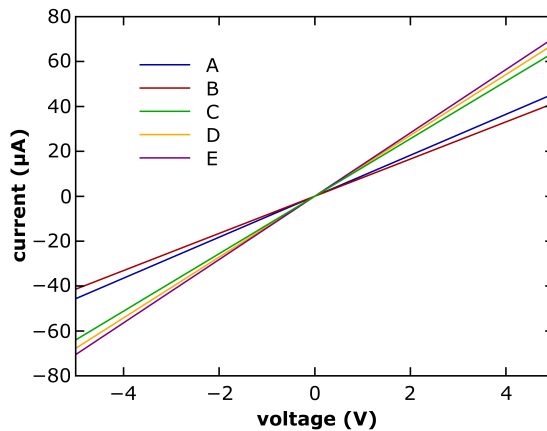


Figure S4: Current-voltage (IV) data of the as-deposited 6DT cross-linked GNP films A, B, C, D and E. The data are normalized to an electrode geometry with a channel length of 400 μ m and channel width of 1 cm.

Resonator Microstructure

The left hand side of Figure S5 depicts a schematic of the electrode microstructure used for device fabrication prior to membrane transfer. The image shows the global top electrode (signal ground) and the local back electrodes suitable for addressing each of the 16 resonator devices individually. The right hand side of Figure S5 shows a photograph of a resonator contacted using wire bonding (back electrodes) and silver paint (top electrode).

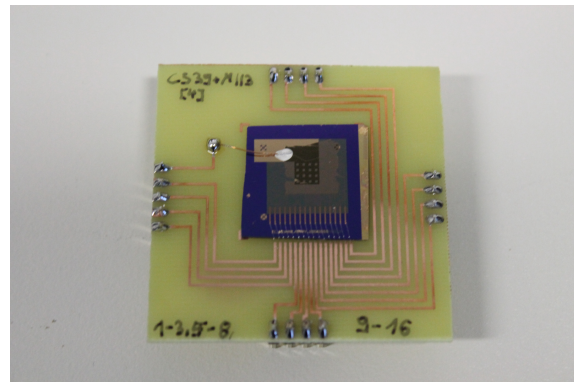
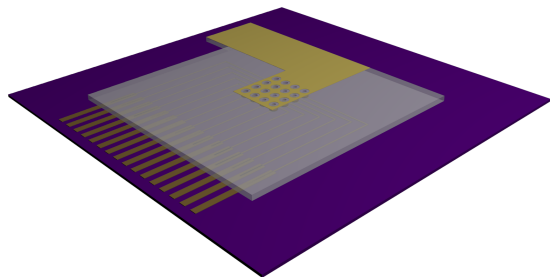


Figure S5: (left) Schematic showing a 3D electrode microstructure prior to GNP membrane deposition. (right) Photograph of a resonator microstructure, after depositing the cross-linked GNP membrane, mounted onto a printed circuit board.

Data Acquisition Procedures

Interferometry

Time dependent deflection series were recorded using a SIOS Nanovibration Analyzer NA (SIOS GmbH, Germany). This instrument is a commercially available, modified Michelson interferometer, working with a 632.8 nm HeNe laser, combined with an optical microscope. The interferometer's optics and detection system provide two electronic signals to the evaluation electronics, representing the sample's deflection as a sine as well as a cosine modulated voltage V_x and V_y , with a periodicity of $\lambda/2$, each. This principle enables the computation of the angle $\theta = \arctan(\frac{V_y}{V_x})$, which linearly corresponds to the sample deflection h . Employing this measurement principle with a precise 90° phase shift between V_x and V_y obtained by waveplates and using matched preamplification and evaluation circuitry, the interferometer enables highly linear deflection measurements. Under the worst conditions the manufacturer expects a cyclic linearity error of less than 3 nm. Typical errors are smaller.

Typically, a laser power of roughly $\sim 5 \mu\text{W}$ was used for the interferometric measurements (spot diameter $< 2 \mu\text{m}$) to avoid destruction of the GNP membranes.

”Frequency Scanning” Spectrum Acquisition

The ”frequency scanning” acquisition method was used to record vibrational spectra of the resonator devices. Here the vibration's amplitudes at continuous drive signals were measured using an interferometric vibration analyzer (SIOS Nanovibration Analyzer NA). Using an Agilent 33521B function generator, a sine voltage signal was generated and amplified by a high-voltage amplifier (Falco Systems WMA-300) with a gain of $G \sim 50$ (eq. S1). The output of the amplifier was connected to the resonator device, which was placed in a vacuum cell. The signal used for driving the resonators was characterized by the drive frequency f_d ,

an amplitude V_{AC} and offset voltage V_{DC} .

$$V(t) = V_{DC} + V_{AC} \sin(2\pi f_d t) \quad (S1)$$

After setting the function generator to the first drive frequency f_d , the interferometer was armed and triggered by the sync signal of the function generator. Receiving a trigger signal, a deflection-time trace $h_{f_d}(t)$ containing 8192 data points measured at a sample rate of 12.5 MHz was recorded. After the measurement was finished, the data were transferred to the measurement computer and the function generator was set to the next drive frequency f_d and the next deflection time trace was recorded. Common vibrational spectra were acquired in a spectral range of 10 kHz to 2 MHz in 1000 steps.

For data analysis, the complex Fourier components at the drive frequencies $C(f_d)$ were computed from the deflection-time traces $h_{f_d}(t)$ acquired at the respective drive frequencies following equation S2:

$$C(f_d) = \frac{1}{T} \int_0^T h_{f_d}(t) e^{i2\pi f_d t} dt \quad (S2)$$

Here, T denotes the length of the $h(t)$ time trace. The data analysis was conducted using Python, and for the numerical integration numpy's `trapz` algorithm was applied. Finally, the amplitude spectrum was obtained by computing the magnitudes of the complex Fourier components:

$$h_0(f_d) = 2|C(f_d)| \quad (S3)$$

Also the phase spectrum of the vibration could be extracted by computing the phase of the complex Fourier coefficients:

$$\phi(f_d) = \angle C(f_d) \quad (S4)$$

However, an interpretation of the phase data was omitted as the phase spectrum was affected by phase shifts caused by the high voltage amplifier.

”Frequency Sweeping” Spectrum Acquisition

The ”frequency sweeping” spectrum acquisition method enables a fast spectrum acquisition, e.g. for determination of the fundamental resonance frequencies or amplitude mappings. Here, the devices are again driven using a sine voltage signal as described in the preceding section. However, in case of the ”frequency sweeping” acquisition, the frequency of the drive signal f_d is linearly swept through the frequency range of interest by the function generator while a deflection time trace is recorded by the interferometer, synced with the beginning of the sweep. Commonly, deflection time traces $h(t)$ with 65536 points were recorded at a sampling frequency of 5 MHz. This resulted in a sweep time of $t_s \sim 13.1$ ms. The recorded time traces $h(t)$ were then transformed to the frequency domain by a custom Python routine employing numpy’s `fft` algorithm to yield the amplitude spectrum.

Amplitude Mapping Acquisition

GNP membrane resonators with a diameter of 100 μm were investigated regarding the spatial deflection amplitude distributions of the membrane during the excitation of different vibrational modes. As the mode frequencies slightly shifted absolutely and relatively upon scanning the membrane with the interferometer laser, vibrational spectra of the membrane were acquired at each x, y mapping position. Usually, the membranes were scanned following a 41×41 grid, spanning $110 \times 110 \mu\text{m}^2$ around the center of the membrane. To avoid scanning large portions of the substrate, data points were only recorded at grid positions having a distance of $\leq 55 \mu\text{m}$ to the membrane center.

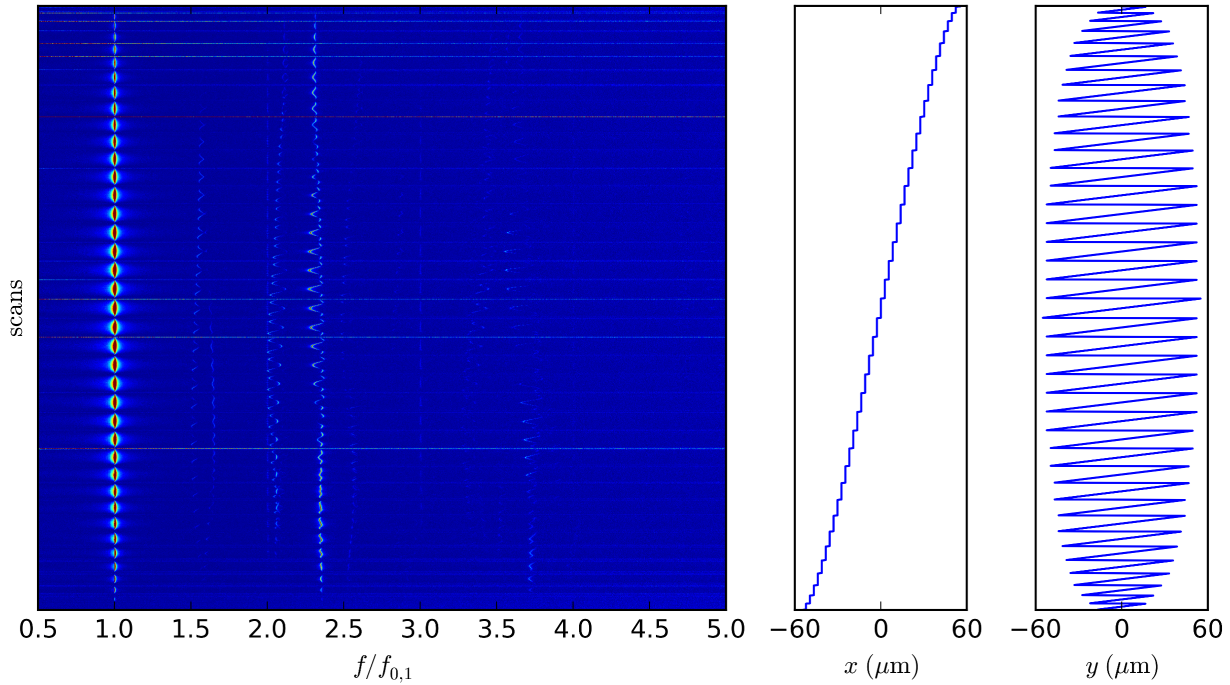


Figure S6: Normalized membrane vibration amplitude spectra recorded at different coordinates ($x = 0, y = 0$ represents the center of the membrane), normalized to the fundamental resonance frequency $f_{0,1}$. Each line represents a scan at the x, y position given in the plots on the right hand side of the figure.

At each position, an amplitude spectrum of the membrane's oscillation in a frequency range of 0.1 to 2 MHz was recorded applying the "frequency sweeping" spectrum acquisition method. The spectra were then normalized to the fundamental resonance frequency $f_{0,1}$.

Figure S6 depicts the normalized vibration spectra recorded for computing the amplitude maps shown in Figure 4 of the main document. Each line in figure S6 represents the spectrum recorded at the x, y -position given by the plots on the right hand side of the figure. For generating the amplitude maps, the peak amplitudes measured at $f_{0,1}$ and in the ranges $2.20f_{0,1} < f < 2.40f_{0,1}$ as well as $3.50f_{0,1} < f < 3.80f_{0,1}$ were plotted at their respective spatial coordinates as false-color images (figure 4). The frequency ranges used for this purpose were chosen around the estimated mode frequencies $f_{0,2;est} = 2.30f_{0,1}$ and $f_{0,3;est} = 3.60f_{0,1}$.

Ring Down Experiments

For determining the resonators quality factors Q , the devices were excited with a burst of a sine voltage signal as described by equation S1 extending over 10, 20, 30, 40, 50 and 80 cycles. The interferometric deflection measurement was synced with the beginning of the excitation burst. Usually, 65536 $h(t)$ datapoints were recorded with a sampling frequency of 12.5 MHz, 10 MHz or 5 MHz.

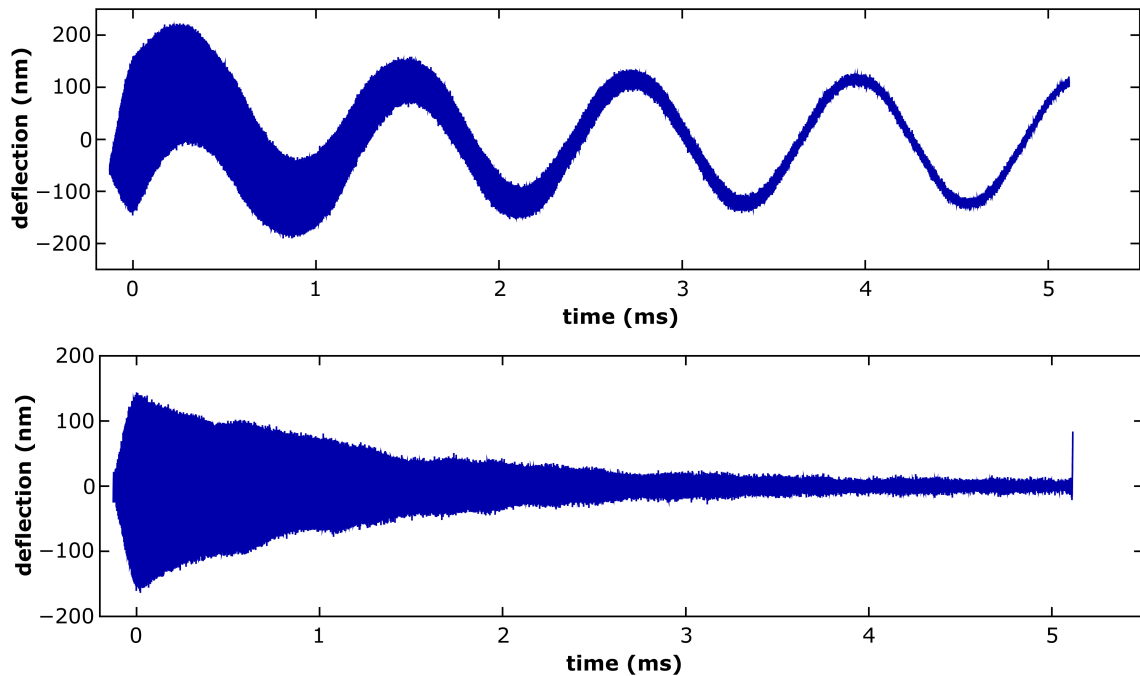


Figure S7: (top) Raw deflection data obtained from a ring-down experiment. (bottom) Deflection data after removal of the modulation caused by the oscillation of the the interferometer's reference mirror.

Figure S7, top, depicts the raw deflection data used for plotting the deflection time traces shown in figure 5 (excitation ends at $t = 0$). A modulation of the data with a frequency of ~ 800 Hz, which is caused by the periodic movement of the interferometer's reference mirror, is clearly visible. This low-frequency modulation was removed by Fourier transformation of the data to the frequency domain using a Python routine employing numpy's `rfft` algorithm, setting the Fourier components in the frequency range ≤ 100 kHz to zero and back-transformation to the time domain applying numpy's `irfft` routine. The result-

ing high-pass filtered deflection trace is depicted in figure S7, bottom. The excitation of the resonator until $t = 0$ is clearly visible, followed by a decay of the oscillation. We note that after the major decay of the vibration, low amplitude vibrations slowly running out of phase, presumably due to thermal excitation, could be observed. These oscillations did not affect our quality factor determinations within the given error margin of sample-to-sample fluctuations. The processed deflection data were fitted with equation S5 as described in the main document using `scipy's optimize.curve_fit` algorithm. As initial optimization parameters, f_{res} was set to the excitation frequency, h_0 and τ were chosen as 10 nm and 1 ms, respectively. A phase value of $\phi = 3.14$ was chosen. In rare cases, ϕ had to be adjusted to achieve conversion of the fitting procedure.

$$h(t) = h_0 \sin(2\pi f_{res}t + \phi) \exp\left(-\frac{t}{\tau}\right) \quad (\text{S5})$$

Variation of DC and AC Voltages

In general, the "frequency sweeping" spectrum acquisition was used for the determination of the resonator's fundamental resonance frequencies. DC offset voltages of $V_{DC} = 5$ V with an AC drive voltage of $V_{AC} = 2.5$ V were applied for devices consisting of a 100 μm resonator and $V_{DC} = 10$ V and $V_{AC} = 5$ V were used for driving 50 μm resonators.

In order to investigate the dependence of the resonance frequency on the offset voltage a 100 μm resonator was examined at a constant AC drive voltage of $V_{AC} = 5$ V and a varying DC offset voltage V_{DC} in the range from 5 V to 20 V.

Also, the possible variation of the resonance frequency in relation to a varying AC drive voltage was studied. For a 100 μm resonator the AC drive voltage V_{AC} was varied in a range from 1.25 V to 3.75 V at a constant DC offset voltage of $V_{DC} = 6.25$ V. Analogously, for a 50 μm resonator an AC drive voltage V_{AC} ranging from 1.25 V to 5 V with a DC offset voltage of $V_{DC} = 6.25$ V was applied.

Neither the variation of the DC offset voltage nor the AC drive voltage in the given ranges resulted in a resonance frequency shift distinguishable from the frequency drifts due to thermal effects caused by the incident laser beam.

Summary of the Resonator Characteristics

26 resonators built from 6DT cross-linked GNP membranes were investigated in this study. The membrane diameters $2a$, membrane thicknesses t , fundamental resonance frequencies $f_{0,1}$ and quality factors Q are listed in table S1.

Table S1: Parameters of resonators investigated in this study. a is the resonator's membrane radius, t denotes the membrane thickness as determined by AFM, $f_{0,1}$ is the fundamental resonance frequency as measured using the "frequency sweeping" spectrum aquisition method and Q denotes the quality factor measured by ring-down experiments.

device	$2a/\mu\text{m}$	t/nm	$f_{0,1}/\text{kHz}$	Q
A1	100	33 ± 2	403.5	2068
A2	100		351.6	779
A3	50		732.2	802
B1	100	35 ± 1	356.4	1769
B2	100		381.9	1737
B3	100		385.3	1491
B4	100		382.7	1371
B5	100		371.8	543
B6	50		738.4	926
C1	100	51 ± 1	325.2	1433
C2	50		625.2	441
C3	50		728.5	850
C4	50		733.7	692
C5	50		617.8	931
C6	50		638.4	1028
C7	50		740.5	1017
C8	50		727.6	927
D1	100	52 ± 1	374.5	1385
D2	100		330.7	803
D3	100		362.7	1164
D4	50		697.2	737
D5	50		691.0	634
D6	50		769.0	584
E1	100	51 ± 1	353.2	1265
E2	100		310.4	1101
E3	100		298.2	1125

References

- (1) Schlicke, H.; Schröder, J. H.; Trebbin, M.; Petrov, A.; Ijeh, M.; Weller, H.; Vossmeyer, T. Freestanding films of crosslinked gold nanoparticles prepared via layer-by-layer spin-coating. *Nanotechnology* **2011**, *22*, 305303.
- (2) Schlicke, H.; Battista, D.; Kunze, S.; Schröter, C. J.; Eich, M.; Vossmeyer, T. Free-standing Membranes of Cross-Linked Gold Nanoparticles: Novel Functional Materials for Electrostatic Actuators. *ACS Appl. Mater. Interfaces* **2015**, *7*, 15123–15128.
- (3) Joseph, Y.; Besnard, I.; Rosenberger, M.; Guse, B.; Nothofer, H.-G.; Wessels, J. M.; Wild, U.; Knop-Gericke, A.; Su, D.; Schlögl, R. et al. Self-Assembled Gold Nanoparticle/Alkanedithiol Films: Preparation, Electron Microscopy, XPS-Analysis, Charge Transport, and Vapor-Sensing Properties. *J. Phys. Chem. B* **2003**, *107*, 7406–7413.